Available online at www.sciencedirect.com
SCIENCE DIRECT®
Thermochimica Acta 411 (2004) 43–51
thermochimica acta
www.elsevier.com/locate/tca

Determination of unfrozen matrix concentrations at low temperatures using stepwise DSC

Jens Liesebach [a,*], Miang Lim [a], Thomas Rades [b]

[a] *Department of Food Science, University of Otago, Dunedin, New Zealand*
[b] *School of Pharmacy, University of Otago, Dunedin, New Zealand*

Received 25 March 2003; received in revised form 30 June 2003; accepted 21 July 2003

Abstract

The aim of the current study was to determine whether stepwise DSC (SW-DSC) is a suitable method for measuring the unfrozen matrix concentration (C_g) of binary aqueous solutions at temperatures as low as −50 °C. The optimal experimental conditions were determined using water. Reliable heat capacity values were determined at nominal scanning rates between 10 and 100 K min^{-1}, sample weights between 8 and 15 mg, and with the sample completely covering the base of the DSC pan. These conditions were then applied to aqueous solutions of ethylene glycol, glycerol and sodium chloride.

The apparent heat is the sum of all heat including latent heat, heat capacity and heat of dilution. The influence of each term on the apparent heat was discussed in detail. The apparent heat values of the frozen samples were then used to calculate the ice fraction in the solution and were expressed as the C_g. The calculated C_g values were similar to previously published values. This study showed that SW-DSC can be used to determine the C_g over a wide temperature range using only one single solution. This technique is advantageous for solutes that are not available in large quantities.

Keywords: Stepwise DSC; Unfrozen matrix concentration; Melting curve; Ethylene glycol; Glycerol; Sodium chloride

1. Introduction

When an aqueous solution is cooled below its freezing temperature, ice can form. The formation of ice removes water from the solution and concentrates the solutes in the unfrozen matrix (UFM). This increase in solute concentration has been shown to increase the kinetics of various types of reactions [1,2], cause precipitation of solutes [3–5] and, in the case of biological samples, influence the cell survival rate during frozen storage [6,7]. The UFM concentration (C_g) can be determined from freezing or melting curves, which are generated by techniques, such as cryoscopy [8,9], differential scanning calorimetry (DSC) [10,11], differential thermal analysis [4,12] and refractometric measurements [13]. A common feature of these methods is that only one freezing/melting temperature can be measured per solute concentration, therefore solutions with a wide range of initial concentrations must be prepared and then analyzed. Furthermore, solutions of high solute concentrations may impede ice formation, which prevents accurate measurement of freezing temperatures [14–16].

Continuous scanning DSC (CS-DSC) has been widely used to determine the melting temperature of frozen matrices [10,11]. This technique records the energy involved in the transition, however, the progressing temperature scan may not allow sufficient time for phase transitions to reach equilibrium and could cause a time lag [17,18]. Because of this time lag, the recorded phase transition temperature is affected by factors, such as scanning rate, sample weight, type of matrix and the heat conductivity of the pan and the sample. To minimize the time lag, slow scanning rates and small sample weights are used. This troublesome lag can also be reduced by using stepwise DSC (SW-DSC), in which the sample temperature is alternated in a series of heating and isothermal steps. The adjustable isothermal steps provide sufficient time for the phase transition to occur and thus the energy of a transition can be measured at steady state conditions [18]. The heat required to change the temperature

* Corresponding author. Tel.: +64-3-479-5463; fax: +64-3-179-7567.
E-mail address: jens_liesebach@gmx.de (J. Liesebach).

0040-6031/$ – see front matter © 2003 Elsevier B.V. All rights reserved.
doi:10.1016/j.tca.2003.07.005

by one heating step is equivalent to the area under the peak of the heat flow versus time curve. This heat represents the sum of all heat values including the latent heat, heat capacity and heat of dilution and is called the apparent heat.

When the apparent heat of a frozen solution is known, the ice fraction in the frozen matrix can be calculated, based on the assumption that the apparent heat is a function of the energy required to heat the molecules and melt ice. Ice melting is a first order transition involving a large quantity of heat. For instance, the energy required to melt 1 g of ice is approximately 80 times larger than the energy required to heat 1 g of water [19] by 1 K, and approximately 160 times larger than the energy required to heat 1 g of ice [19] or 1 g of solute [20,21] by 1 K. The heat of dilution is usually disregarded as its value is small compared to the latent heat of ice [18,22]. The heat capacity of supercooled water has been shown to increase dramatically at low temperatures [23]. However, the heat capacity of binary solutions containing more than 35% water did not show this increase at the same temperature range as the water appears to be closely associated with the solute [24,25].

The temperature dependency of the latent heat of ice can be calculated at constant pressure using Eq. (1) [26]:

$$\Delta H_{\mathrm{lat}(T)} = \Delta H_{\mathrm{lat}(T_0)} - \int_{T_0}^{T} (C_{p(\mathrm{l})} - C_{p(\mathrm{s})})\,\mathrm{d}T \quad (1)$$

where dT is the temperature difference between the melting temperature of pure water and the temperature of interest, $\Delta H_{\mathrm{lat}(T_0)}$ and $\Delta H_{\mathrm{lat}(T)}$ are the latent heat values for ice at the melting temperature of pure water and the temperature of interest, and $C_{p(\mathrm{l})}$ and $C_{p(\mathrm{s})}$ are the heat capacity values of water and ice, respectively. At temperatures close to 0 °C, the latent heat and the heat capacity can be considered to be constant, although they are temperature dependent.

The SW-DSC has only been applied in one previous study to determine the C_g at temperatures as low as −13 °C [18]. However, no details were given about the latent heat and heat capacity values used for the calculation of C_g. The aim of the current study was to determine whether SW-DSC is a suitable method for measuring the C_g of binary aqueous solutions at temperatures as low as −50 °C. The optimal experimental conditions were determined using water and then applied to aqueous solutions of ethylene glycol, glycerol and sodium chloride (NaCl).

2. Method

The thermodynamic properties were measured using DSC (Pyris 1, Perkin Elmer, USA). Samples were sealed in pre-weighed aluminum pans (24.50 ± 0.04 mg) and the sample weight was confirmed after each scan. The temperature of the DSC was calibrated with water (>99.994%, Aldrich, USA) and indium (>99.99%, Perkin Elmer, USA). The onset of the melting peaks at scanning rates between 0.5 and 20 K min^{-1} was measured and extrapolated to a scanning rate of 0 K min^{-1} using a linear trendline, therefore representing the onset of the transitions at isothermal conditions.

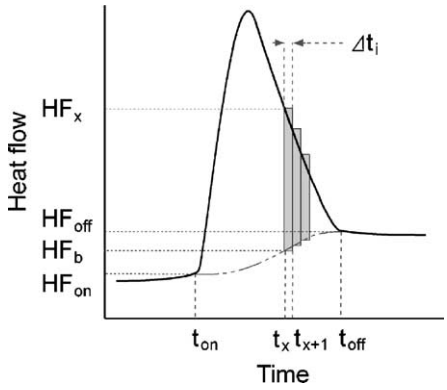

Fig. 1. Summary of the terms used for the calculation of the area under the peak.

The stepwise temperature program consisted of a series of alternating 1 K heating steps and isothermal steps. The length of the isothermal steps was adjusted to allow sufficient time for reaching steady state conditions, and ranged from 2 to 25 min. When the heat flow was plotted against time, the area under the peaks represented the heat required to increase the temperature at each step.

The area under each peak was calculated using software designed by the authors. The terms used for calculation of the area under the peak are illustrated in Fig. 1. This software determined the peak onset and offset from five consecutive first derivative values, where the sum of these values exceeded 0.33. The peak onset and offset times were confirmed by visual observations. The offset of tailing peaks at step temperatures close to the melting temperature and at a nominal scanning rate at 1 K min^{-1} were adjusted manually.

A sigmoidal baseline under the peak (HF_b) was required as the difference between the heat flow of the peak onset (HF_{on}) and offset (HF_{off}) increased by approximately 0.1 mW per step. The shape of the baseline was determined by the time difference between the peak onset (t_{on}) and offset (t_{off}), and the amplitude was adjusted by the heat flow difference between the peak onset and offset (Eq. (2)). The sum of the heat flow values for the sigmoidal baseline and the peak onset represents the HF_b:

$$\mathrm{HF_b} = \tfrac{1}{2}[\cos[(\pi/(t_{\mathrm{off}} - t_{\mathrm{on}}))(t_{\mathrm{off}} - t_x)] + 1] \times (\mathrm{HF_{off}} - \mathrm{HF_{on}}) + \mathrm{HF_{on}} \quad (2)$$

where t_x is the time between t_{on} and t_{off}. The area under the peak was segmented into small rectangles, where the width was the time difference between two recorded heat flow values ($\Delta t_i = 0.2$ s) and the height was calculated by the difference between the recorded heat flow (HF_x) and HF_b at t_x. The sum of the area of each rectangle represented

the total area under the peak (A) as shown in the following equation:

$$A = \sum_{x=t_{on}}^{t_{off}} (\Delta t_i)(HF_x - HF_b) \quad (3)$$

In order to convert the area under the peak into energy, a calibration factor (F) was calculated using the ratio of the theoretical apparent heat and the difference in the area under the peak between a DSC pan with water and an empty DSC pan, (Eq. (4)). The theoretical apparent heat includes the energy required to heat the sample before and after the transition using the heat capacity of ice and water [27], and the heat required to melt the ice using the latent heat of ice [27]:

$$F = \frac{m_w C_{p(s)}(T_{Tr} - T_1) + m_w C_{p(l)}(T_2 - T_{Tr}) + m_w \Delta H_{lat}}{A_w - A_b} \quad (4)$$

where m_w is the weight of the water sample, ΔH_{lat} the latent heat of ice, T_{Tr} the transition temperature, T_1 and T_2 are the start and end temperatures of the heating step, A_w and A_b the areas under the peak of a DSC pan loaded with water and an empty DSC pan, respectively. The energy required to heat the solution by one step was calculated by first multiplying the area for the solution with the calibration factor, and then normalized to the apparent heat of the solution (ΔH_{app}) by dividing it by the sample weight (m_s) (Eq. (5)):

$$\Delta H_{app} = \frac{F(A - A_b)}{m_s} \quad (5)$$

The optimal experimental conditions for the SW-DSC method were determined using water samples (>99.994%, Aldrich, USA) at various nominal scanning rates, sample weights and sample coverage of the base of the DSC pan. These conditions were then applied to binary solutions of ethylene glycol (99%, freshly opened, Aldrich, USA), glycerol (>99.9%, freshly opened, Sigma, USA) or NaCl (BDH, England) mixed with de-ionized water, that was passed through a water purifier (Millipore, USA). The solutions (12.6 ± 1.6 mg) were evenly distributed in the DSC pans and analyzed using SW-DSC at a nominal scanning rate of $80\,K\,min^{-1}$. Each result was based on at least three scans, and the overall coefficient of variation for the baseline was less than 0.2%.

The ice fraction in the frozen samples was calculated from the apparent heat values between the step temperature and melting temperature. The equation used to calculate the ice fraction was adapted from literature [18] to include the temperature dependent latent heat, heat capacity values and the heat of dilution (Eq. (6)):

$$\Delta H_{app} = y_1 \Delta H_{lat} + (y_2 C_{p(s)} + x C_{p(sol)} + [1 - y_2 - x] C_{p(l)})(T_2 - T_1) + \Delta H_{dil} \quad (6)$$

where $C_{p(sol)}$ is the heat capacity of the solute, ΔH_{dil} the heat of dilution, y_1 the ice fraction formed between T_1 and T_2, and y_2 and x are the weight fractions at T_2 of ice and solute, respectively.

Sodium chloride solutions were also analyzed using CS-DSC at $5\,K\,min^{-1}$. The calibration settings from the SW-DSC calibration were applied since CS-DSC and SW-DSC were operated alternately. The experimental melting temperatures of ice and indium were elevated at 0.15 and 0.18 K compared to the reference values [28], respectively. Literature values for the latent heat, heat capacity and freezing temperatures were fitted using a fourth order polynomial (Excel, Microsoft, USA).

3. Results and discussion

The first part of this study investigated the influence of the experimental conditions on the heat capacity of ice and water in order to optimize the SW-DSC method. The optimal experimental conditions were used to determine the apparent heat of aqueous binary solutions, then the heat capacity and latent heat terms in Eq. (6) were discussed. Finally, the ice fraction was calculated using the apparent heat, and expressed as the C_g.

3.1. Optimization of the SW-DSC method

Analysis of the thermodynamic properties using DSC depends on the operating conditions and the sample properties. The influence of the scanning rate, sample weight and sample coverage of the DSC pan base on the heat capacity values of ice and water were studied. A typical SW-DSC scan of water is shown in Fig. 2. Each peak represented a temperature step of 1 K. In the absence of any phase transition, sharp peaks with a width of approximately 60 s were

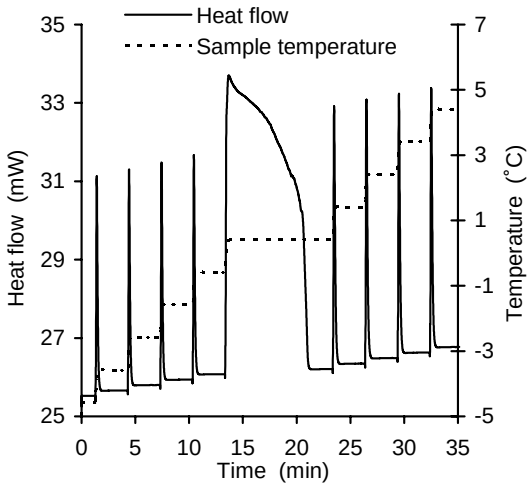

Fig. 2. SW-DSC scan of an 8 mg water sample at temperatures between −4.5 and 4.5 °C recorded at a nominal scanning rate of $80\,K\,min^{-1}$. The irregular peak between 13 and 23 min indicated ice melting.

observed, however, when the temperature step involved a transition, such as ice melting, the shape of the peak was irregular and the width increased with sample size.

It was assumed that the scanning rate would have no effect on the heat involved at each step since the length of the isothermal step would allow sufficient time to reach steady state conditions. In order to confirm this assumption, the influence of the scanning rate was investigated by varying the nominal scanning rate. The nominal scanning rate refers to the rate of heat input and does not necessarily reflect the actual scanning rate as the DSC requires time to achieve fast scanning rates, for instance a nominal scanning rate above 20 K min^{-1} would need less than 3 s to heat through a temperature range of 1 K, but approximately 60 s were required to complete the heating step in a SW-DSC scan at a nominal scanning rate of 100 K min^{-1}. At five nominal scanning rates ranging from 1 to 100 K min^{-1}, the calibration factors were constant ($F = 0.9882 \pm 0.0005$ J mm^{-2}), but the shape of the peaks was affected. Sharp peaks were recorded at nominal scanning rates above 10 K min^{-1} and were easily detected by the peak analysis software. Broad peaks with gradual offsets were recorded at a nominal scanning rate of 1 K min^{-1} and led to unreliable offset measurements using the automatic routine of the peak analysis software. As a result, the offset of these peaks had to be determined manually.

Experimental heat capacity values of ice at a nominal scanning rate of 1 K min^{-1} were higher than values at nominal scanning rates between 10 and 100 K min^{-1} (Fig. 3). It was also observed that as the temperature increased, the heat capacity values gradually increased and then at temperatures close to 0 °C the gradient became noticeably steeper. The opposite was observed at temperatures above 0 °C, where the heat capacity values decreased with an increase in temperature (Fig. 4), but as for the heat capacity values of ice, the highest values were recorded at a nominal scanning rate of 1 K min^{-1}. These observations

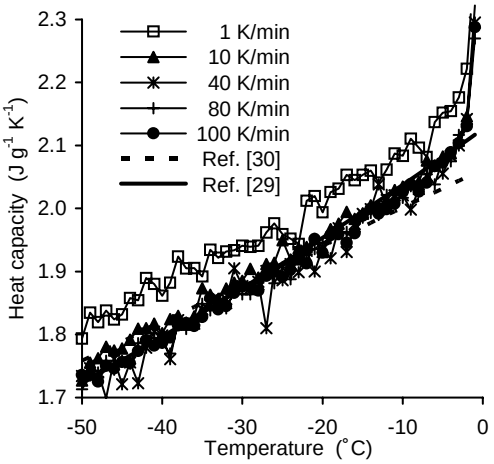

Fig. 3. Heat capacity values of ice determined at nominal scanning rates between 1 and 100 K min^{-1}. Sample weight was 8 mg. Values from literature are included for comparison.

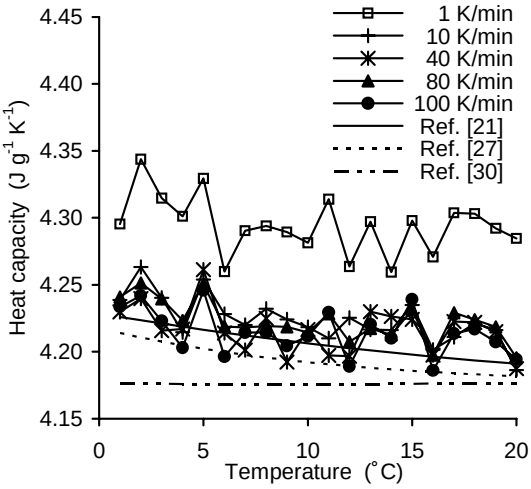

Fig. 4. Heat capacity values of water determined at nominal scanning rates between 1 and 100 K min^{-1}. Sample weight was 8 mg. Values from literature are included for comparison.

showed that when the nominal scanning rate is between 10 and 100 K min^{-1}, the SW-DSC consistently measures the heat capacity.

The effect of sample weight was investigated by analyzing the calibration factor and the heat capacity values of ice and water at a nominal scanning rate of 80 K min^{-1} (Fig. 5). A consistent calibration factor was obtained for 8–15 mg water, but outside this range, lower values were obtained (inset of Fig. 5). The overall trends for the heat capacity of ice and water were similar to those of a previous study performed at different scanning rates (Figs. 3 and 4). Heat capacity values of water samples weighing less than 4 mg were lower than the heat capacity values for samples weighing 4 mg or more. Outside the weight range between 8 and 15 mg, deviations of the calibration factors were observed, which may have been due to differences in the sample shape and

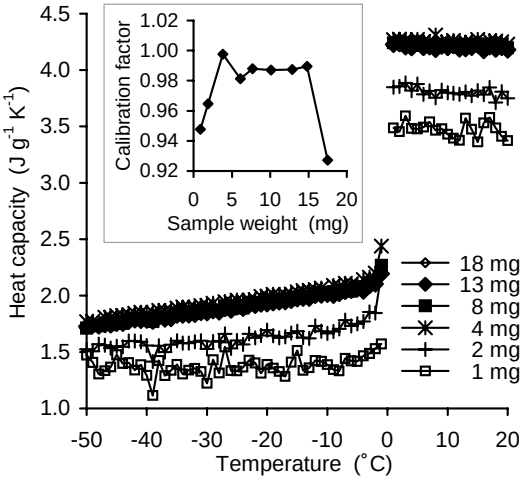

Fig. 5. Heat capacity values of ice and water with the sample weight ranging from 0.9 to 17.5 mg. Inset: calibration factor versus sample weight. The nominal scanning rate was 80 K min^{-1}.

sample position. Depending on the surface tension, small samples are likely to form droplets, where the diameter of the center of the droplet would be larger than the base of the droplet that was in contact with the base of the DSC pan. In contrast, larger samples are more likely to cover the entire base of the DSC pan, thus resulting in reproducible contact areas. In this study, approximately 8 mg of sample were necessary to cover the entire base of a DSC pan. Larger sample weights would only increase the height of the sample, although this may affect the heat transfer within the sample as the calibration factor for the 17.5 mg sample was lower than for the samples between 8 and 15 mg.

The effect of the sample shape was investigated using two samples of approximately 8 mg of water that either partially or completely covered the base of the DSC pan. The variation in the degree of coverage did not affect the calibration factor or melting temperature, but the heat capacity values of the sample that only partially covered the base were lower than samples that completely covered the base. When 3 mg of water was placed on the inside of the DSC pan lid, the ice melting temperature was unaffected, however, the calibration factor ($0.994\,J\,mm^{-2}$) was slightly higher than the calibration factor determined for the 4 mg sample that was placed on the base of DSC pan, and the heat capacity values were the lowest reported for the entire study. From these observations, it was concluded that complete coverage of the base of the DSC pan resulted in more reliable values than a partially covered base.

Most of the ice melted in one step, although slightly higher heat capacity values for ice above $-2.5\,^{\circ}C$ indicated that melting occurred below $0\,^{\circ}C$ (Figs. 3 and 5). This may be an artifact of the DSC, which was also shown in a previous study [18]. In a DSC, the energy necessary to heat the sample is provided from the heating element below the sample. Therefore, heat is supplied to the sample through the base of the DSC pan. This is likely to cause a temperature gradient within the sample. At temperatures well below the transition, the energy input is not sufficient to melt ice at the base, but when the temperature is close to the melting temperature of ice, it is possible that the heat supplied exceeds the energy level and only a small fraction of ice melts at the base. The additional heat increase for an 8 mg sample at $80\,K\,min^{-1}$ was equivalent to approximately 0.05% melted ice at 1 K below the melting step. Another reason for the increased heat capacity values of ice could have been due to small quantities of impurities in the water. The certificate of analysis for the water used stated that there were 0.006% impurities. This meant that 0.006 g of solute were dissolved in 0.05 g of unfrozen water at $-1.5\,^{\circ}C$ and therefore, the concentration of the impurities in the UFM was 11%. A UFM concentration of 11% at $-1.5\,^{\circ}C$ has also been observed with other solutes [27], which supports the idea that the increase in the heat capacity of ice could also be due to the impurities in the water used.

In general, the experimental heat capacity values of ice were similar to previously published data by Handa et al. [29] and Lide [19], but the slope of the heat capacity values differed slightly from Choi and Okos [30]. The experimental heat capacity values for water were similar to the values reported by Perry and Green [21], but were approximately $0.05\,J\,g^{-1}\,K^{-1}$ higher than values obtained by Choi and Okos [30] and Weast [27]. This suggested that the heat capacity of a sample can be determined reliably at nominal scanning rates between 10 and $100\,K\,min^{-1}$, sample weights between 8 and 15 mg, and with the sample completely covering the base of the DSC pan.

3.2. Apparent heat of aqueous binary solutions

The apparent heat of the aqueous binary solutions was measured at temperatures between -50 and $10\,^{\circ}C$. The nominal scanning rate was $80\,K\,min^{-1}$, the weight of the samples was between 10 and 14 mg, and the samples completely covered the base of the DSC pans. The SW-DSC scans were started 25 and 15 K above the glass transition of the maximally freeze-concentrated ethylene glycol solution [31] and glycerol solution [31,32], respectively. These temperatures were chosen to avoid the high viscosity at temperatures close to the glass transition of the UFM, which can hinder ice formation [33]. Furthermore, the SW-DSC scans were only started when the heat flow was constant and therefore, it was assumed that the ice formation in ethylene glycol and glycerol solutions was close to steady state conditions at the starting temperature.

Typical apparent heat versus temperature curves for frozen solutions were obtained for both the ethylene glycol and the glycerol solutions (illustrated for ethylene glycol in Fig. 6). The apparent heat values increased moderately at very low temperatures before they peaked, dropped sharply,

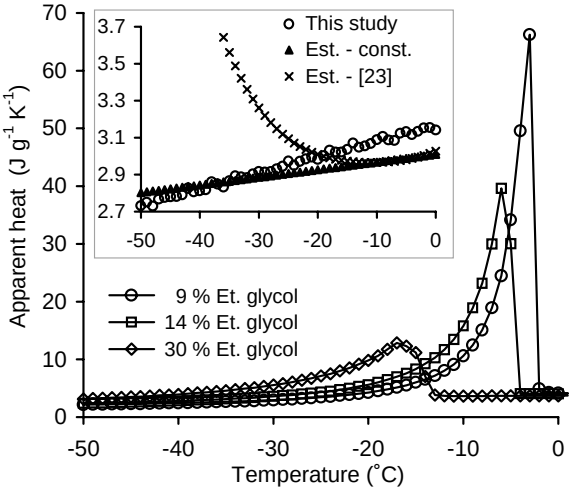

Fig. 6. Apparent heat of ethylene glycol solutions with initial concentrations ranging between 9 and 30%. Inset: apparent heat of a 60% ethylene glycol solution. The apparent heat values were determined using SW-DSC. The estimated apparent heat values shown in the inset (Est.) were calculated using heat capacity values of water from either a constant value of $4.2\,J\,g^{-1}\,K^{-1}$ [19] or literature [23] (see text).

Table 1
Linear equations describing the heat capacity and apparent heat capacity values at low temperatures

	Heat capacity ($J\,g^{-1}\,K^{-1}$)	Reference
Solute		
Ethylene glycol	$0.0055T + 2.2454$[a]	[20]
Glycerol	$0.0052T + 2.2461$[a]	[21]
NaCl	$0.185 + 0.000072(273 + T) \times 0.07164$[a]	[21]
	Apparent heat capacity ($J\,g^{-1}\,K^{-1}$)	R^2
Solution		
59.9% ethylene glycol	$0.0084T + 3.161$[a]	0.995
64.8% glycerol	$0.0076T + 3.010$[a]	0.995
NaCl, lower transition		
Peak at −22.5 °C	$0.260S + 2.115$[b]	0.978
Peak at −21.5 °C	$10.430S + 0.419$[b]	0.999

[a] T is the temperature (°C).
[b] S is the initial NaCl concentration (%).

and then leveled off between 3 and $4\,J\,g^{-1}\,K^{-1}$. Ethylene glycol and glycerol solutions with an initial concentration above 59% did not freeze and the apparent heat followed a linear trendline (Fig. 6 and Table 1). The apparent heat values of ethylene glycol solutions compared favorably with the values determined by Huot et al. [34] ($0.08\,J\,g^{-1}\,K^{-1}$) and by Nan et al. [20] ($0.12\,J\,g^{-1}\,K^{-1}$), when the literature values were interpolated based on the nearest pair at temperatures between 0 and 10 °C. Frozen glycerol solutions at temperatures between −30 and 2 °C had apparent heat values close to the values reported by Gucker and Marsh [25] ($0.10\,J\,g^{-1}\,K^{-1}$), although the slope of the 65% solution deviated by $0.0086\,J\,g^{-1}\,K^{-2}$.

The power versus temperature plot of NaCl solutions was similar to the melting scans of ethylene glycol and glycerol, but an additional transition was observed that was split into two steps at −22.5 and −21.5 °C (Fig. 7). This transition has been identified as the NaCl–water eutectic, where a matrix of 22.42% NaCl crystallizes to NaCl dihydrate and ice [35]. In the current study, NaCl solutions were not annealed at −21 °C because of the eutectic and therefore, it is likely that the freezing process did not achieve the maximally freeze-concentrated UFM.

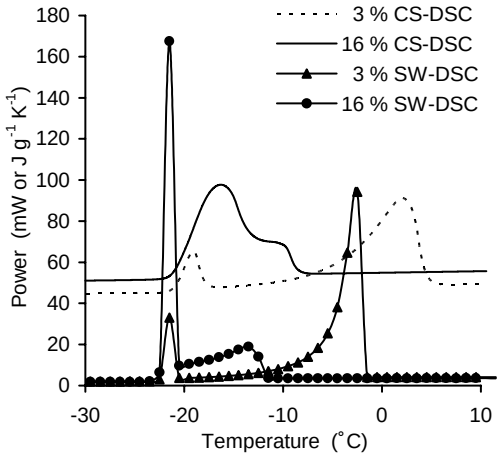

Fig. 7. Power versus temperature plot of a 3 and 16% NaCl solution using SW-DSC and CS-DSC at a heating rate of $5\,K\,min^{-1}$. The apparent heat from the SW-DSC is given in $J\,g^{-1}\,K^{-1}$ and the heat flow from the CS-DSC in mW.

The latent heat of the eutectic for three different initial NaCl concentrations (3, 10, 16%), as determined using SW-DSC, was well described by linear trendlines (Table 1). According to these trendlines, an aqueous 22.42% NaCl solution should have a latent heat of $242\,J\,g^{-1}$. This was confirmed by a SW-DSC scan of a 22.44% NaCl solution, which had a latent heat of $244\,J\,g^{-1}$. These values were close to the latent heat of $250\,J\,g^{-1}$ for a 22.42% NaCl solution that had been determined previously using CS-DSC [3]. It should be emphasized that the latent heat of the NaCl–water eutectic was measured at low initial NaCl concentrations with ice present. This was only achievable because the adjustable isothermal step allowed sufficient time for the transition to occur. In contrast, CS-DSC scans revealed several transitions at temperatures between −21 and 4 °C, which depended on the initial NaCl concentration (Fig. 7). The 3% NaCl solution showed two broad peaks, but for the 16% NaCl solution, peak separation was not successful as the two transitions merged. Analysis of the scans revealed that the SW-DSC always recorded lower transition temperatures than those recorded in the CS-DSC even before temperature correction. The temperature lag of CS-DSC was especially obvious in the 3% NaCl solution, where the ice melting peak was completed above 4 °C (Fig. 6). At temperatures between 0 and 10 °C, the apparent heat values of the NaCl solutions were larger than the values reported by Washburn [36] ($0.05\,J\,g^{-1}\,K^{-1}$), which were interpolated based on the nearest pair.

3.3. Apparent heat and latent heat of ice

The apparent heat is the sum of all heat including latent heat, heat capacity and heat of dilution. The heat of dilution caused only a small difference in heat in the system compared to the heat required for melting [37–39], therefore it was not included in the following calculations, but is discussed at the end of the paper. It was assumed that mixing was ideal.

Heat capacity values of ice were obtained from literature because the experimentally determined values in the first part of this study were similar to the values reported by Handa et al. [29]. The heat capacity values for the solutes were obtained from literature [20,21] and extrapolated to the temperature range of interest (Table 1). To our knowledge, the heat capacity value for unfrozen water in the UFM has not been previously determined. The applicability of heat capacity values of pure unfrozen water [23] was studied using ethylene glycol and glycerol solutions with a high initial solute concentration. The estimated apparent heat values for an ethylene glycol and glycerol solution was a

non-linear function of temperature and diverged from the experimental values at low temperatures when heat capacity values from literature were used [23] (inset of Fig. 6). On the other hand, the experimental apparent heat values of solutions with high initial solute concentrations increased linearly with temperature (Fig. 6 and Table 1). A similar trend was also observed for a 60% glycerol solution at temperatures between −30 and 5 °C [25]. Since both the experimental apparent heat and the heat capacity of the solutes increased linearly with temperature, the heat capacity values for the unfrozen water must be either linear or constant. Furthermore, it was shown that the anomaly of bulk water, i.e. the increase in heat capacity of supercooled water at low temperatures [23], was removed for a solution with 18.6% hydrogen peroxide at temperatures between −70 and 0 °C [24]. For the following calculations of the latent heat and C_g, the heat capacity of unfrozen water was considered to be that of water at 0 °C (4.2 J g^{-1} K^{-1} [19]).

The latent heat of ice depends on the temperature [40–42]. This should also apply to water in highly concentrated matrices, such as the UFM, although bulk water is likely to behave differently. Therefore, Eq. (6) was rearranged to calculate the latent heat of ice in frozen matrices using the heat capacity as described above and freezing points from literature [3,9,27]. The calculated latent heat of ice obtained from binary solutions at various initial concentrations followed a non-linear pattern (Fig. 8). In general, the latent heat of ice increased as the temperature increased. The values for the last melting step were not included since the last ice crystals melted in between the SW-DSC heating step.

The latent heat values of ice in this study were of the same magnitude as literature values, but the shape of the lines differed significantly [40–42]. This may be due to the type of trendline used to calculate the C_g curve. For this reason, the latent heat values for two different sets of freezing points for ethylene glycol were calculated and compared (Fig. 8). Both latent heat curves had a similar shape, however, the values varied by up to 14%. This indicated that the freezing curves used had a large impact on the latent heat values at the lower end of the temperature scale [9,27]. Another possible reason for the differences between the latent heat values may be that the samples had not reached steady state. When the heating step starts, heat is supplied to the base of the sample through the DSC pan, therefore, it is likely that ice melting begins at the base of the sample. This caused a loss in sample uniformity as the ice could now float in the upper part of the denser UFM. The additional layer of UFM between the DSC pan and ice could then have decreased the rate of reaching steady state since water has a lower heat conductivity than ice. Before the steady state was achieved, the next heating step had begun and the previously unfinished melting transition was carried over to the following step. This could explain why the latent heat values of ice above −10 °C were smaller than at temperatures of approximately −20 °C.

Overall, ice melting may not always occur at steady state conditions, but most of the ice melted at conditions close to steady state. For the calculation of the C_g, the temperature dependency of the latent heat of ice was calculated using Eq. (1) and the specific heat values of water [19] and ice [29], which described the experimentally determined latent heat sufficiently (Fig. 8).

3.4. Calculation of UFM concentration

The C_g of frozen ethylene glycol, glycerol and NaCl solutions were calculated from the apparent heat using Eq. (6), where the heat capacity and latent heat values used were as mentioned above. The heat of dilution was considered to be negligible. The C_g of various ethylene glycol solutions were similar at high freezing temperatures (Fig. 9). The standard deviation, however, increased with a decrease in the temperature from 0.5% at −15 °C to 2.5%

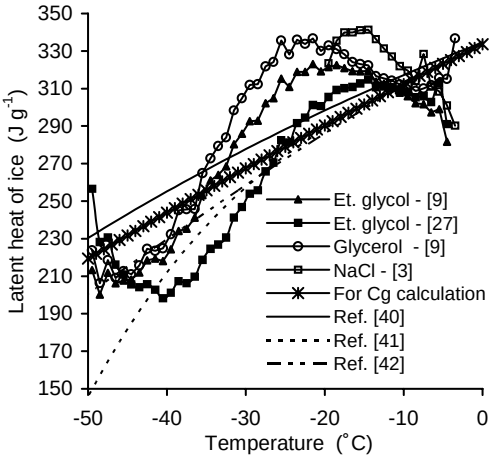

Fig. 8. Temperature dependency of latent heat values for ice as determined in this study and literature. References stated after the solutes indicate the source of the freezing temperatures used for the calculation of the latent heat of ice.

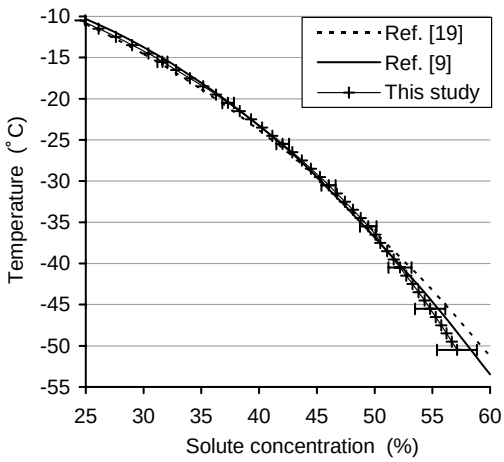

Fig. 9. C_g values of ethylene glycol solutions in this study and values from literature. The standard deviation of five solutions with initial concentrations of 4, 9, 14, 30 and 46% is illustrated at 5 K intervals.

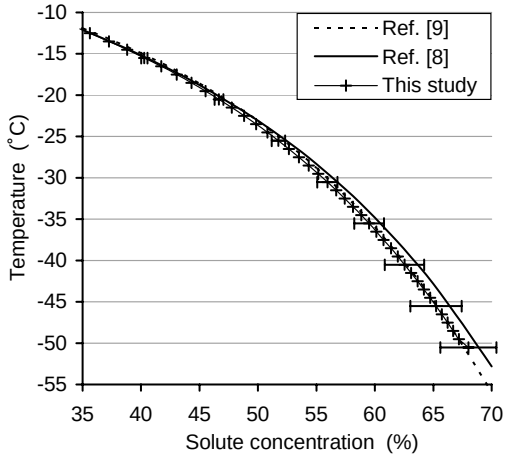

Fig. 10. C_g values of glycerol solutions in this study and values from literature. The standard deviation of four solutions with initial concentrations of 5, 9, 15 and 30% is illustrated at 5 K intervals.

at −50 °C. This may be caused by the accumulative method that was used to calculate the ice fraction, starting first at the melting temperature and then towards lower temperatures. The average C_g of the five different initial ethylene glycol concentrations was close to literature values [9,12,27,43] (Fig. 9). Similar results were observed for four different glycerol solutions (Fig. 10), where the experimental C_g values were close to previously reported values [8,9,12,44].

Two transitions were observed when NaCl solutions were heated from −50 to 10 °C. The first transition at low temperatures was the melting of the eutectic phase and the second transition was the melting of ice [3,45]. The average C_g of three different initial NaCl concentrations resulted in an overall C_g that was higher than previously reported [3,27,35] (Fig. 11), however, the highest standard deviation was only 1.0%.

For the calculations of the C_g, the mixing of the solutes and water was considered to be ideal, although small

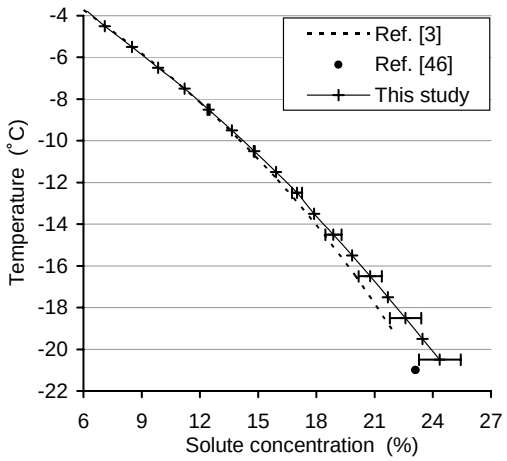

Fig. 11. C_g values of NaCl solutions in this study and values from literature. The standard deviation of three solutions with initial concentrations of 3, 10 and 16% is illustrated at 5 K intervals.

Table 2
C_g values determined in this study and from literature

Solute	Calculation	C_g at −50.5 °C	
		This study (%)	Literature (%)
Ethylene glycol	Without heat of dilution	57.1 ± 1.7	58.3 [9], 59.5 [27], 60.1 [43], 62.2 [12]
	With heat of dilution	56.4 ± 1.3	
Glycerol	Without heat of dilution	68.0 ± 2.4	68.8 [8], 67.6 [9]
	With heat of dilution	67.1 ± 2.3	
		C_g at −21.5 °C	
		This study (%)	Literature (%)
NaCl	Without heat of dilution	24.2 ± 1.0	22.4 [35], 23.1 [46]
	With heat of dilution	23.8 ± 0.8	

quantities of excess energy were measured when mixing the two components at 25 °C [37–39]. The C_g were again calculated using Eq. (6), but this time literature values for the heat of dilution at 25 °C [37–39] were taken into account (Table 2). The results show that the heat of dilution only had a minimal effect on the C_g and was insignificant compared to the standard deviation of the C_g curves and thus, the heat of dilution was disregarded. A similar conclusion was reached by other authors [18,22].

4. Conclusion

The SW-DSC enabled the C_g to be determined at temperatures as low as −50 °C. Validation of the system indicated that a nominal scanning rate above 1 K min^{-1} and an evenly distributed sample weight between 8 and 15 mg resulted in reliable values. The experimentally determined heat capacity values of ice and water samples were in good agreement with literature. The optimal experimental conditions were applied to determine the apparent heat of frozen aqueous solutions of ethylene glycol, glycerol and NaCl. The SW-DSC scans were also compared to the CS-DSC scans and it was observed that the SW-DSC recorded sharper transitions and lower transition temperatures.

The apparent heat values of the frozen solutions were used to calculate the ice fraction, which was expressed as C_g. The C_g values compared well with previously published values. This study showed that SW-DSC can be used to determine the C_g over a wide temperature range using only one single solution. This is advantageous for solutes that are not available in large quantities.

Acknowledgements

The authors thank J.E. McFetridge for her assistance in the preparation of the manuscript.

References

[1] R. Shija, V.B. Sunderland, C. McDonald, Int. J. Pharm. 80 (1992) 203.
[2] N.H. Grant, H.E. Alburn, Science 150 (1965) 1589.
[3] M. Jochem, C. Koerber, Cryobiology 24 (1987) 513.
[4] M.L. Shepard, C.S. Goldston, F.H. Cocks, Cryobiology 13 (1976) 9.
[5] R.K. Cavatur, R. Suryanarayanan, Pharm. Res. 15 (1998) 194.
[6] H. Yang, J.P. Acker, J. Hannon, H. Miszta-Lane, J.J. Akabutu, L.E. McGann, Cytotherapy 3 (2001) 377.
[7] W. De Loecker, V.A. Koptelov, V.I. Grischenko, P. De Loecker, Cryobiology 37 (1998) 103.
[8] L.B. Lane, Ind. Eng. Chem. 17 (1925) 924.
[9] H.K. Ross, Ind. Eng. Chem. 46 (1954) 601.
[10] E.J. Woods, M.A.J. Zieger, D.Y. Gao, J.K. Critser, Cryobiology 38 (1999) 403.
[11] I. Arvanitoyannis, J.M.V. Blanshard, S. Ablett, M.J. Izzard, P.J. Lillford, J. Sci. Food Agric. 63 (1993) 177.
[12] B. Luyet, D.H. Rasmussen, Biodynamica 10 (1968) 167.
[13] G. Steinbach, Sci. Tech. Froid, 1977, p. 53.
[14] H.D. Goff, M.E. Sahagian, Thermochim. Acta 280 (1996) 449.
[15] S. Ablett, M.J. Izzard, P.J. Lillford, J. Chem. Soc., Faraday Trans. 88 (1992) 789.
[16] S. Ablett, M.J. Izzard, P.J. Lillford, I. Arvanitoyannis, J.M.V. Blanshard, Carbohydr. Res. 246 (1993) 13.
[17] D.S. Reid, J. HSU, W. Kerr, in: J.M.V. Blanshard (Ed.), The glassy state in foods, Nottingham University Press, 1993, 123 pp.
[18] W. Kerr, D.S. Reid, Thermochim. Acta 246 (1994) 299.
[19] D.R. Lide, CRC Handbook of Chemistry and Physics, CRC Press, Boca Raton, FL, 2002.
[20] Z. Nan, B. Liu, Z. Tan, J. Chem. Thermodyn. 34 (2002) 915.
[21] R.H. Perry, D.W. Green, Perry's Chemical Engineer's Handbook, McGraw-Hill, New York, 1997.
[22] R.H.M. Hatley, C. van den Berg, F. Franks, Cryo-Letters 12 (1991) 113.
[23] C.A. Angell, J. Shuppert, J.C. Tucker, J. Phys. Chem. 77 (1973) 3092.
[24] M. Oguni, C.A. Angell, J. Chem. Phys. (1980) 31.
[25] F.T. Gucker Jr., G.A. Marsh, Ind. Eng. Chem. 40 (1948) 908.
[26] S. Glasstone, Textbook of Physical Chemistry, Macmillan, London, 1962.
[27] R.C. Weast, M.J. Astle, W.H. Beyer, CRC Handbook of Chemistry and Physics, CRC Press, Boca Raton, FL, 1989.
[28] Perkin-Elmer, Pyris 1-Manual, Temperature Calibration Standards, 2000.
[29] Y.P. Handa, R.E. Hawkins, J.J. Murray, J. Chem. Thermodyn. 16 (1984) 623.
[30] Y. Choi, M.R. Okos, in: M. Le Maguer, P. Jelen (Eds.), Food Engineering and Process Applications, Elsevier, London, 1986, 93 pp.
[31] H. Levine, L. Slade, Cryo-Letters 9 (1988) 21.
[32] B.S. Chang, C.S. Randall, Cryobiology 29 (1992) 632–656.
[33] Y.H. Roos, Phase Transitions in Foods, Academic Press, London, UK, 1995.
[34] J.Y. Huot, E. Battistel, R. Lumry, G. Villeneuve, J.F. Lavallee, A. Anusiem, C. Jolicoeur, J. Solution Chem. 17 (1988) 601.
[35] Landolt-Börnstein, Gleichgewichte ausser Schmelzgleichgewichte, Springer-Verlag, Berlin, 1962.
[36] E.W. Washburn, International Critical Tables of Numerical Data in Physics, Chemistry and Technology, McGraw-Hill, New York, 1929.
[37] E.E. Messikomer, R.H. Wood, J. Chem. Thermodyn. 7 (1975) 119.
[38] Y. Marcus, Phys. Chem. Chem. Phys. 2 (2000) 4891.
[39] Y. Matsumoto, H. Touhara, K. Nakanishi, N. Watanabe, J. Chem. Thermodyn. 9 (1977) 801.
[40] E.W. Hansen, H.C. Gran, E.J. Sellevold, J. Phys. Chem. B 101 (1997) 7027.
[41] F. Franks, Water—A Comprehensive Treatise, Plenum Press, New York, 1985.
[42] C.S. Chen, Trans. ASAE 31 (1988) 1602.
[43] D.R. Cordray, L.R. Kaplan, P.M. Woyciesjes, T.F. Kozak, Fluid Phase Equilib. 117 (1996) 146–152.
[44] S. Budavari, The Merck Index, Merck & Co., Withehouse Station, NJ, 1996.
[45] E.Y. Shalaev, F. Franks, Thermochim. Acta 255 (1995) 49.
[46] D.G. Archer, J. Phys. Chem. Ref. Data 21 (1992) 793.